

Transitioning from MODIS to VIIRS: an analysis of inter-consistency of NDVI data sets for agricultural monitoring

Sergii Skakun ^{a,b}, Christopher O. Justice ^a, Eric Vermote ^b, Jean-Claude Roger ^{a,b}

^a *Department of Geographical Sciences, University of Maryland, College Park, MD, USA*

^b *NASA Goddard Space Flight Center Code 619, Greenbelt, MD, USA*

Correspondence author details:

Sergii Skakun

Department of Geographical Sciences, University of Maryland, College Park, MD
20740, USA

NASA Goddard Space Flight Center Code 619, 8800 Greenbelt Road, Greenbelt, MD
20771, USA

Address: 4321 Hartwick Road, Suite 400, College Park, MD 20740, USA

E-mail: skakun@umd.edu; sergii.skakun@nasa.gov

Tel: +1-301-614-5084

Transitioning from MODIS to VIIRS: an analysis of inter-consistency of NDVI data sets for agricultural monitoring

The Visible/Infrared Imager/Radiometer Suite (VIIRS) aboard the Suomi National Polar-orbiting Partnership (S-NPP) satellite was launched in 2011, in part to provide continuity with the Moderate Resolution Imaging Spectroradiometer (MODIS) instrument aboard National Aeronautics and Space Administration's (NASA) Terra and Aqua remote sensing satellites. The VIIRS will eventually replace MODIS for both land science and applications and add to the coarse-resolution, long term data record. It is, therefore, important to provide the user community with an assessment of the consistency of equivalent products from the two sensors. For this study, we do this in the context of example agricultural monitoring applications. Surface reflectance that is routinely delivered within the M{O,Y}D09 and VNP09 series of products provide critical input for generating downstream products. Given the range of applications utilizing the normalized difference vegetation index (NDVI) generated from M{O,Y}D09 and VNP09 products and the inherent differences between MODIS and VIIRS sensors in calibration, spatial sampling, and spectral bands, the main objective of this study is to quantify uncertainties related the transitioning from using MODIS to VIIRS-based NDVI's. In particular, we compare NDVI's derived from two sets of Level 3 MYD09 and VNP09 products with various spatial-temporal characteristics, namely 8-day composites at 500 m spatial resolution and daily Climate Modelling Grid (CMG) images at 0.05° spatial resolution. Spectral adjustment of VIIRS I1 (red) and I2 (near infra-red — NIR) bands to match MODIS/Aqua b1 (red) and b2 (NIR) bands is performed to remove a bias between MODIS and VIIRS-based red, NIR, and NDVI estimates. Overall, red reflectance, NIR reflectance, NDVI uncertainties were 0.014, 0.029 and 0.056 respectively for the 500 m product and 0.013, 0.016 and 0.032 for the 0.05° product. The study shows that MODIS and VIIRS NDVI data can be used interchangeably for applications with an uncertainty of less than 0.02 to 0.05, depending on the scale of spatial aggregation, which is typically the uncertainty of the individual dataset.

Keywords: MODIS; S-NPP VIIRS; NDVI; inter-comparison; agriculture

1. Introduction

The Moderate Resolution Imaging Spectroradiometer (MODIS) aboard the Terra and Aqua remote sensing satellites has been successfully imaging the Earth's surface since 2000 and 2002, respectively. With spatial resolutions of 250 m, 500 m and 1 km and 36 spectral bands, MODIS provides temporal composites and daily images with near real-time access to data (Davies *et al.* 2015) that are critical to many applications. The portfolio of the MODIS-based land products has been expanding and improving through 5 Collections, to include surface reflectance (SR), vegetation indices (VIs), biophysical parameters (leaf area index and fraction of absorbed photosynthetically active radiation), net and gross primary productivity, bidirectional reflectance distribution function (BRDF), albedo, temperature and land cover.

Surface reflectance that is delivered within the MODIS series of products (Vermote and Kotchenova 2008) provides a critical input for generating such downstream products and needs to be of the highest possible quality, so that minimal uncertainties propagate in the dependent/downstream products. An important downstream product is the normalized difference vegetation index (NDVI). NDVI has been one of the most important and widely applicable VI's dating back to the Advanced Very High Resolution Radiometer (AVHRR) instruments aboard National Oceanic and Atmospheric Administration (NOAA) satellites (Justice *et al.* 1985), and is used in various agricultural applications including crop yield prediction (Becker-Reshef *et al.* 2010a; Franch *et al.* 2015, 2017; Johnson 2016; Kogan *et al.* 2014; Meroni *et al.* 2016), crop mapping (Chang *et al.* 2007; Pittman *et al.* 2010; Skakun *et al.* 2017; Xiao *et al.* 2005), crop calendar and phenology analysis (Sakamoto *et al.* 2010; Whitcraft *et al.* 2015), and drought monitoring and crop state assessment (AghaKouchak *et al.* 2015; Gu *et al.* 2007; Karl *et al.* 2012). More importantly, VIs derived from MODIS surface

reflectance products have been integrated into operational agricultural monitoring systems at global, national and regional scales (Becker-Reshef *et al.* 2010b). With the MODIS Terra sensor already experiencing degradation (Wang *et al.* 2012), it is advisable to establish continuity observations for these applications.

The Visible/Infrared Imager/Radiometer Suite (VIIRS) aboard the Suomi National Polar-orbiting Partnership (S-NPP) satellite was launched in 2011 and was planned to provide continuity with MODIS (Justice *et al.* 2013). VIIRS images the Earth's surface in 22 spectral bands at 375 m (I bands) and 750 m (M bands) spatial resolution. A series of VIIRS-based surface reflectance products VNP09, analogous to the M{O,Y}D09 suite, is being routinely generated (Vermote *et al.* 2014) using the same approach for atmospheric correction as for MODIS (Vermote and Kotchenova 2008; Vermote *et al.* 2002). VIIRS will eventually replace MODIS for both land science and applications and add to the coarse-resolution, long term data record. It is therefore, important to provide the user community with an assessment of the consistency of equivalent products from the two sensors. For this study, we do this in the context of example agricultural monitoring applications. Previous studies have provided some insight into continuity and inter-comparison issues between MODIS and VIIRS using simulated data (Fan and Liu 2016; Kim *et al.* 2010; Van Leeuwen *et al.* 2006; Miura *et al.* 2013), top-of-atmosphere (TOA) NDVI and top-of-canopy (TOC) enhanced vegetation index (EVI) (Fan and Liu 2017; Obata *et al.* 2016; Vargas *et al.* 2013) and AERONET-based validation (Shabanov *et al.* 2015). Given the range of applications utilizing NDVI generated from M{O,Y}D09 and VNP09 products and the inherent differences between MODIS and VIIRS instruments in terms of calibration, spatial sampling and spectral bands, the main objective of this study is to quantify uncertainties related to transitioning from MODIS to VIIRS based NDVI's. In particular, we compare

NDVI derived from two sets of Level 3 products (MYD09 and VNP09) with different spatial-temporal characteristics. For this study, we selected: (i) 8-day composited products at 500 m spatial resolution, as composited data are commonly used in agricultural applications to minimize the impact of cloud cover and (ii) daily Climate Modelling Grid (CMG) images at 0.05° spatial resolution, as increasingly, daily data are being used to avoid losing high temporal frequency good observations eliminated by temporal compositing (Franch *et al.* 2017). The comparison is performed particularly for the MYD09 products, with similar afternoon overpass times from Aqua and S-NPP satellites (i.e. 13:30 local time).

2. Surface Reflectance Products M{O,Y}D09 and VNP09

The M{O,Y}D09 (Vermote *et al.* 2015) and VNP09 (Roger *et al.* 2016) products suites provide an estimate of the surface spectral reflectance for the corresponding MODIS and VIIRS spectral bands, as would have been measured at ground level if there were no atmospheric scattering or absorption. The same atmospheric correction algorithm which uses the Second Simulation of a Satellite Signal in the Solar Spectrum, Vector (6SV) radiative transfer code and internal algorithm for aerosol retrieval is applied to both MODIS and VIIRS (Vermote *et al.* 2014; Vermote and Kotchenova 2008). Corrections are made for the effects of molecular gases, including ozone and water vapour, and for the effects of atmospheric aerosols.

M{O,Y}D09 is a seven-band product computed from the MODIS Level 1B bands 1 to 7. VNP09 is a twelve-band product computed from the Land SIPS V1 Level 1B bands I1–I3, M1–M5, M7, M8, M10, and M11. Both M{O,Y}D09 and VNP09 include daily Level 2G (L2G) data, that have been mapped to the sinusoidal grid, and Level 3 (L3) data, that have been spatially and/or temporally aggregated. Table 1 and 2

provide details on Level 2G and Level 3 products from the M{O,Y}D09 and VNP09 series.

[Table 1 near here]

[Table 2 near here]

For the temporal compositing process, each pixel containing the single best possible L2G observation during an 8-day period (hereafter referred as ‘best pixel’) is selected on the basis of high observation coverage, low sensor angle, the absence of clouds or cloud shadow, and aerosol loading. For spatial aggregation to CMG grid, an area weighted average of the best quality observations from the L2G product is used. The CMG product also provides the number of 250 m (for bands 1-2) and 500 m (for bands 3-7) best quality pixels which were used for averaging at 0.05° spatial resolution.

3. Methodology

NDVI products from MODIS and VIIRS at different spatial and temporal resolution were compared in this study. In particular, the comparison was performed on a per-pixel basis for MYD09 and VNP09 products at 500 m and 0.05° (CMG) resolution, respectively. No aggregation (within a window) was performed for either resolution as the goal was to compare products at their ‘native’ resolutions. Bands b1 (red) and b2 (near infra-red (NIR)) from MODIS and I1 (red) and I2 (NIR) from VIIRS were used to calculate the NDVI using a standard formula (Tucker 1979): $(NDVI) = (\rho_{NIR} - \rho_{red}) / (\rho_{NIR} + \rho_{red})$, where ρ_{NIR} and ρ_{red} are surface reflectance values in NIR and red spectral bands, respectively. The VIIRS I1 and I2 bands were used instead of M5 and M7 bands for the CMG product because the spectral response functions from the I bands are more similar to those from MODIS, especially in the red (Figure 1).

[Figure 1 near here]

The 500 m 8-day composite product, comparison was performed for four tiles of the MODIS sinusoidal grid (h10v04, h10v05, h11v04 and h11v05), covering the Midwest US (Corn Belt, Figure 2), which is a major agricultural production region in the U.S.

[Figure 2 near here]

Though MODIS/Aqua and VIIRS sensors image the Earth's surface at approximately the same time of day, the day of the year (DOY) within an 8-day period, for which the 'best pixel' value is selected for MYD09A1 and VNP09A1 products, might be different. Therefore, only the same DOY observations were used for comparison. In addition, only close to nadir observations from both sensors, i.e. with view zenith angle (VZA) less than 7.5° , were considered to reduce the effects of spatial resolution and BRDF.

A comparison of CMG products, namely MYD09CMG and VNP09CMG, was performed globally for land pixels. Daily MODIS and VIIRS CMG products exhibit different viewing geometries, and therefore BRDF correction is necessary to normalize the surface reflectance values. For this, we applied the VJB algorithm (Vermote *et al.* 2009) for both MODIS/Aqua and VIIRS. The surface reflectance values in red and NIR bands from MODIS and VIIRS were normalized to the $(45^\circ, 0^\circ)$ solar and viewing angles:

$$\rho^N(45,0,0) = \rho(\theta_s, \theta_v, \varphi) \frac{1 + VF_1(45,0,0) + RF_2(45,0,0)}{1 + VF_1(\theta_s, \theta_v, \varphi) + RF_2(\theta_s, \theta_v, \varphi)}, \quad (1)$$

where θ_s is the solar zenith angle; θ_v is the sensor VZA; φ is the relative azimuth angle; F_1 is the volume scattering kernel, based on the Ross thick function, but corrected for the Hot-Spot process; F_2 is the geometric kernel, based on the Li-sparse reciprocal function; V and R are free parameters that are estimated for each pixel at CMG resolution using the BRDF inversion technique. We refer the reader to (Vermote *et al.* 2009) for the details of the VJB algorithm implementation.

Since MODIS and VIIRS spectral response functions in red and NIR bands exhibit differences (Figure 1), corresponding spectral adjustments should be performed to reduce differences in red, NIR and NDVI estimates derived from MODIS and VIIRS sensors. In this study, surface reflectance values from VIIRS were adjusted to those of MODIS/Aqua. For this, corresponding relationships between red and NIR bands from MODIS and VIIRS were developed using the following equations:

$$\rho_{\text{red}}^{\text{M}} = a_{\text{red}}\rho_{\text{red}}^{\text{V}} + b_{\text{red}}\rho_{\text{NIR}}^{\text{V}}, \quad (2)$$

$$\rho_{\text{NIR}}^{\text{M}} = a_{\text{NIR}}\rho_{\text{red}}^{\text{V}} + b_{\text{NIR}}\rho_{\text{NIR}}^{\text{V}}, \quad (3)$$

where $\rho_{\text{red}}^{\text{M}}$, $\rho_{\text{NIR}}^{\text{M}}$, $\rho_{\text{red}}^{\text{V}}$, $\rho_{\text{NIR}}^{\text{V}}$ are surface reflectance values in red and NIR for MODIS (superscript M) and VIIRS (superscript V), and a_{red} , b_{red} , a_{NIR} , b_{NIR} are conversion coefficients estimated from data using the ordinary least squares (OLS) regression. Note that these relationships are without the constant term to ensure that ‘black’ surfaces have the same reflectance values for both sensors. It is also expected that both the sums of coefficients, namely $a_{\text{red}} + b_{\text{red}}$ and $a_{\text{NIR}} + b_{\text{NIR}}$, will be close to 1 to ensure continuity of reflectance values for ‘bright’ surfaces such as clouds. Spectral adjustment for red and NIR bands for MYD09A1/VNP09A1 (500 m) and MYD09CMG/VNP09CMG (0.05°) products using Equations (2)–(3) was performed on a yearly basis and for the entire period of 2012–2016, to analyse the ‘temporal stability’

of the conversion coefficients.

The NDVI anomaly is another indicator often used to analyse how the current vegetation condition relates to that of the previous years (AghaKouchak *et al.* 2015; Becker-Reshef *et al.* 2010b; Gu *et al.* 2007; Karl *et al.* 2012; Meroni *et al.* 2016). Here, we calculate a multi-year median of NDVI for each pixel from MODIS/Aqua, and combined MODIS/Aqua and adjusted VIIRS at CMG resolution. More specifically, for MODIS/Aqua data sets only, a median NDVI is calculated for 2002–2012. For a combination of MODIS and VIIRS NDVI data, a median NDVI is calculated for a set of NDVI values concatenated from MODIS/Aqua (2002–2011) and adjusted VIIRS (2012–2016). Therefore, we compare two cases: when VIIRS adjusted data, starting from 2012, are used to update the median NDVI values from MODIS/Aqua, and when only MODIS/Aqua is used to calculate the median NDVI (2002–2016):

$$y_{\text{median}}^M = \text{median}(\{y_t^M | t = 2002..2016\}), \quad (4)$$

$$y_{\text{median}}^{MV} = \text{median}(\{y_t^M | t = 2002..2011\}, \{y_t^V | t = 2012..2016\}), \quad (5)$$

where t is the time, expressed here in years, y_t^M and y_t^V are MYD09CMG and VNP09CMG derived NDVI values for MODIS/Aqua and VIIRS (adjusted with Equations (2)–(3)), respectively.

To quantify the differences and uncertainties between MYD09 and VNP09 products and NDVI-derived estimates, a standard *APU* analysis is performed (Vermote and Kotchenova 2008) with the following set of metrics:

- accuracy (A) that shows the average bias between estimates

$$A = \frac{1}{N} \sum_{i=1}^N (y_i^V - y_i^M) \quad (6)$$

- precision (P) that shows repeatability of the estimates

$$P = \sqrt{\frac{1}{N-1} \sum_{i=1}^N (y_i^V - y_i^M - A)^2} \quad (7)$$

- uncertainty (U) that is the root mean square error

$$U = \sqrt{\frac{1}{N} \sum_{i=1}^N (y_i^V - y_i^M)^2} \quad (8)$$

where y_i^V and y_i^M are VIIRS and MODIS derived values (surface reflectance or NDVI), respectively, and N is the number of values to be compared.

4. Results

4.1. Comparison of MYD09A1 and VNP09A1 derived NDVI at 500 m resolution

Figure 3 shows the difference between the DOY selected within the 8-day period for MYD09A1 and VNP09A1 products for all land pixels (excludes water pixels) in tiles h10v04, h10v05, h11v04 and h11v05 for 2012–2016. The same DOY is selected in 35.4% cases; in 55.6% cases, the DOY difference is 1 day or less; and in 31% cases, the DOY difference is 3 to 7 days. Therefore, when utilizing these products jointly, one has to take into account differences in surface reflectance values or derived VI's caused by the DOY selected and possible surface changes within the compositing period.

[Figure 3 near here]

The distribution of MODIS/Aqua VZAs in MYD09A1 and difference between VZAs for MYD09A1 and VNP09A1 products for the four tiles in US and the 2012–2016 period, are shown in Figure 4 and Figure 5, respectively. For MODIS/Aqua VZAs

distribution, in 27.3% cases the VZA is 0° to 10° ; in 35% of cases, VZA is more than 30° which translates to the effective along-scan spatial resolution of more than 850 m (Figure 4). In 38% and 82% of cases, the difference between MODIS/Aqua and VIIRS VZAs within the 8-day composites is within -10° to 10° and -30° to 30° , respectively; in 18%, the absolute difference is more than 30° .

[Figure 4 near here]

[Figure 5 near here]

The results of ‘temporal’ stability of conversion coefficients are presented in Table 3.

[Table 3 near here]

In general, there is a temporal ‘stability’ for coefficients a_{red} and b_{NIR} as the coefficient of variation (CV) is around 1% which is consistent with the calibration performance (Vermote *et al.* 2014). Coefficients b_{red} and a_{NIR} provide a maximum 2% and 6% contribution to the surface reflectance values for red and NIR bands. Less stability is observed for these coefficients, b_{red} and a_{NIR} , with CV of 6.8% and 44.3%, respectively. It should be noted that larger deviations are observed for the initial years of VIIRS operation, namely 2012 and 2013, while relatively better stability is observed for 2014–2016.

The derived coefficients for 2012–2016 (Table 3) were used to adjust red and NIR reflectance values from VIIRS to match the MODIS ones, and compute the NDVI.

Comparisons of the VIIRS and MODIS/Aqua derived NDVI values with and without spectral adjustment are shown in Figure 6 and Figure 7, respectively.

[Figure 6 near here]

[Figure 7 near here]

Spectral adjustment removed the bias between MODIS/Aqua and VIIRS-derived red, NIR and NDVI values (Figure 6 and Figure 7). Overall red reflectance, NIR reflectance and NDVI uncertainties were 0.014, 0.029 and 0.056, respectively, when considering the same day observation pixels (Figure 6). These uncertainties increased to 0.018, 0.034 and 0.064 (a 14% increase), respectively, when the absolute difference between DOY for ‘best pixels’ from MOD09A1 and VNP09A1 products was 3 to 7 days while VZAs for both sensors were less than 7.5° (Figure 8).

[Figure 8 near here]

Uncertainties can be further reduced when NDVI values at 500 m resolution are spatially aggregated. For example, within the agriculture application domain, NDVI is usually averaged over administrative regions to correlate with crop yield values (Becker-Reshef *et al.* 2010a; Franch *et al.* 2015, 2017; Johnson *et al.* 2016; Kogan *et al.* 2014). Figure 9 shows an example of such aggregation: NDVI values derived from MOD09A1 and VNP09A1 products were averaged for Harper County in Kansas (US) for 500 m pixels with a winter wheat proportion larger than 50%. Winter wheat proportions were derived from USDA CDL maps for 2012–2016 (Johnson and Mueller, 2010). The spatial aggregation decreased uncertainties to 0.021 (2.67 times), compared

to a per-pixel (at 500 m) derived uncertainty of 0.056. Spectral adjustment reduced the bias (accuracy) from 0.017 to -0.003.

[Figure 9 near here]

4.2. Comparison of MYD09CMG and VNP09CMG derived NDVI at 0.05° resolution

Table 4 shows the derived coefficients from Equations (2)–(3) of the regressions to adjust VIIRS red (I1) and NIR (I2) surface reflectance values to MODIS using yearly data and the whole 2012–2016 period. Compared to the 500 m products (MYD09A1 and VNP09A1), better temporal ‘stability’ is observed at CMG resolution.

[Table 4 near here]

The conversion coefficients from Table 4 derived for 2012–2016 were used to adjust VIIRS I1 (red) and I2 (NIR) bands and to compute NDVI. Figure 10 shows comparison of daily NDVI values at 0.05° resolution for all land pixels for 2012–2016 (almost 2×10^9 CMG pixels).

[Figure 10 near here]

The spectral adjustment removed the bias between MODIS/Aqua and VIIRS derived NDVI, and the resulting uncertainty for NDVI was 0.032, 1.75 times smaller than for the 500 m products. Uncertainties for red and NIR spectral bands were 0.013 and 0.016, respectively. CMG based data were spatially aggregated over Harper County

to provide a daily NDVI time series for winter wheat (Figure 11). We selected the top 5% purest winter wheat pixels at CMG resolution to calculate NDVI, the same way it was done for the generalized empirical winter wheat yield forecasting model (Becker-Reshef *et al.* 2010a).

[Figure 11 near here]

With aggregation at Harper County scale, both 500 m and CMG products yielded similar uncertainty of 0.022 when comparing MODIS/Aqua and VIIRS derived NDVI values (Figure 9 and Figure 11); however, the CMG derived NDVI time series is much denser thanks to daily observations.

4.3. Comparison of MYD09CMG and VNP09CMG derived NDVI anomalies at 0.05° resolution

Figure 12 shows a comparison of long-term median NDVI values calculated for MODIS/Aqua only (Equation (4)) and a combination of MODIS/Aqua and adjusted VIIRS (Equation (5)) for 2002–2016. Thanks to VIIRS adjustment, the bias is close to zero (-0.003), and the corresponding NDVI uncertainty is 0.03. Comparison of NDVI anomalies derived from BRDF corrected MOD09CMG and VNP09CMG products is shown in Figure 13. The resulting uncertainty was found to be 0.033 at global scale.

[Figure 12 near here]

[Figure 13 near here]

An example of NDVI values and medians for Iowa (US) is shown in Figure 14, and geographical distribution of NDVI anomalies from MODIS/Aqua and VIIRS for the

same region is shown in Figure 15. Figure 15 shows good spatial consistency between and similar spatial patterns for NDVI anomalies computed from MODIS/Aqua and VIIRS sensors.

[Figure 14 near here]

[Figure 15 near here]

5. Discussion

NDVI is a widely used remote sensing based product which is used in several agricultural monitoring applications. Having high-quality long term NDVI data records is extremely important for studying spatiotemporal changes in Earth's surface dynamics. This requires integration of data records from multiple sensors, including MODIS and VIIRS. VIIRS provides continuity to MODIS, and therefore it is important to enable a proper transition between products from these sensors, so the VIIRS based products can be ingested into existing MODIS based applications, and corresponding uncertainties are quantified and known. This study focused on comparing NDVI derived from the MYD09A1/VNP09A1 and MYD09CMG/VNP09CMG surface reflectance products that provide a trade-off in terms of spatial (500 m versus 0.05°) and temporal resolution (8-day versus daily). In particular, MYD09A1 and VNP09A1 provide data at 500 m resolution at the expense of temporal resolution (8-day). Although, through the compositing process, only high-quality pixels are selected, there are several differences between MODIS/Aqua and VIIRS-based products that influence the inter-consistency of the data sets. First and foremost, differences in spectral response functions in red and NIR bands of MODIS and VIIRS sensors (Figure 1) introduce a bias in surface reflectance values and NDVI estimations that can be removed through spectral

adjustments. We found also, that only in 35.4% cases the DOY of the ‘best pixel’ within the 8-day period is the same for MYD09A1 and VNP09A1 products. Uncertainties of MYD09A1 and VNP09A1 derived NDVI values can be increased more than 14% when the difference between DOY increases to 7 days. Differences were also observed in VZAs for ‘best pixels’ in these products. The off-nadir VZAs values introduce two major issues: a reduced effective spatial resolution of MODIS with the increase of VZA (Figure 4) (thanks to the aggregation, this is not the case for VIIRS (Campagnolo *et al.* 2016; Pahlevan *et al.* 2017)), and BRDF effects for both MODIS and VIIRS. Therefore, users are encouraged to take these into consideration when developing applications at ‘native’ 500 m resolution. Overall, the uncertainties between MYD09A1 and VNP09A1 derived red reflectance, NIR reflectance and NDVI estimates at 500 m resolution for the same day and close to nadir ($VZA < 7.5^\circ$) observations for US for 2012–2016 were found to be 0.014, 0.029 and 0.056, respectively, with VIIRS to MODIS/Aqua spectral adjustment.

A better consistency between MODIS/Aqua and VIIRS derived NDVI’s was observed at CMG scale at 0.05° resolution. Comparison of more than 2×10^9 global CMG pixels for 2012–2016 yielded red reflectance, NIR reflectance and NDVI uncertainties of 0.013, 0.016 and 0.032 respectively, after BRDF correction of MYD09CMG and VNP09CMG surface reflectance values with the VJB approach (Vermote *et al.* 2009), and spectral adjustment of VIIRS to MODIS/Aqua. Corresponding conversion coefficients for adjusting BRDF corrected VIIRS I1 (red) and I2 (NIR) bands to MODIS/Aqua b1 (red) and b2 (NIR) bands were calculated and showed good temporal stability within the 2012–2016 period. While the CMG based products provide a lower spatial resolution as compared to the 500 m products, they provide daily data that might be critical to applications, and, as it is shown in this study,

better consistency between MODIS/Aqua and VIIRS with lower uncertainties.

Uncertainties can be further reduced to 0.022 when NDVI values extracted from 500 m or CMG resolution products are spatially aggregated for administrative regions, as the derived NDVI can, for example, be correlated with crop yields (Becker-Reshef *et al.* 2010a; Franch *et al.* 2015, 2017; Johnson *et al.* 2016; Kogan *et al.* 2014).

These results have certain implications when ingesting VIIRS data into existing MODIS-based models for agricultural monitoring, e.g. crop state assessment or crop yield modelling and forecasting. VIIRS data should be spectrally adjusted to match MODIS data, so no bias will propagate into the final estimates. Consider a model with crop yield linearly depending on the MODIS-based NDVI: $y = \alpha * (\text{NDVI})$. Directly applying the VIIRS-based NDVI's without spectral adjustment will result in higher crop yield estimates, since VIIRS-based NDVI is higher than the MODIS/Aqua-based NDVI (Figure 9 and Figure 11). For example, a slope between winter wheat yield (t ha^{-1}) and MODIS-based NDVI for Harper County in Kansas (US) was found to be 5.34 (Becker-Reshef *et al.* 2010a), while the VIIRS-based NDVI's are on average 0.018 higher than the MODIS-based NDVI's (Figure 11). Therefore, in such a case, the VIIRS-based winter wheat yield estimates will be on average 0.1 t ha^{-1} higher than those from MODIS without spectral adjustment.

Even with the bias removed, differences still exist between MODIS and VIIRS derived NDVI's, and quantifying inter-consistency between the sensors can be helpful in providing the final error of estimates for NDVI-based agricultural products. Consider again the example of Kansas (US) where the winter wheat yield model is estimated to have an RMSE error of 0.18 t ha^{-1} or 7% (Becker-Reshef *et al.* 2010a). When applying the VIIRS-based NDVI's to the model, due to the MODIS-VIIRS NDVI uncertainty of 0.022 (Figure 11), the error of winter wheat yield estimates will be

$\sqrt{0.18^2 + (5.34 \times 0.022)^2} = 0.22 \text{ t ha}^{-1}$ or 8.5%. Therefore, inconsistencies between VIIRS and MODIS based NDVI's will lead to the increase of resulting crop yield uncertainties.

In terms of NDVI anomalies, median values are calculated from a sufficiently long data record to identify 'normal' vegetation conditions, but not so long that the land use or cropping system being observed have changed significantly. Figure 16 shows the timeline of the three remote sensing satellites imaging the Earth's surface with an afternoon overpass, that will be used to form the land long term record: MODIS/Aqua, S-NPP and Joint Polar Satellite System (JPSS). It is expected that MODIS/Aqua will continue its nominal operations until 2022 (personal communication, Robert Wolfe, NASA Goddard Space Flight Center, June 2017) and JPSS-1 is planned to be launched at the end of 2017. At the time of writing, MODIS/Aqua has a 15 year data record which is used to calculate the median NDVI value. At the MODIS/Aqua end of life (2022), the data record would be 20 years and the VIIRS/S-NPP record would be 10 years. Inter-use of data products from these sensors is therefore likely to continue to be desirable; however, if the NDVI data records are combined, one should do so with an awareness of NDVI anomaly inter-consistency uncertainties of 0.033.

[Figure 16 near here]

6. Conclusion

The main focus of this study was to quantify uncertainties between MODIS/Aqua and VIIRS based NDVI calculated from the suite of MYD09 and VNP09 products that provide an estimate of surface reflectance, which provides the basis for the NDVI.

Because of differences in spectral response functions in red and NIR bands of MODIS (b1, b2) and VIIRS (I1, I2), there is a bias when comparing MODIS and VIIRS estimates that is removed through a spectral adjustment procedure. Corresponding coefficients were calculated for MYD09 and VNP09 products at 500 m (for US) and CMG (globally) spatial resolution using observations from 2012 to 2016 that can be further used by the user community in their research activities. At 500 m spatial resolution and 8-day temporal resolution, uncertainty between NDVI derived from MODIS/Aqua and VIIRS was 0.056 for the same day and close to nadir observations ($VZA < 7.5^\circ$). For daily BRDF corrected NDVI and NDVI anomalies values at 0.05° resolution, uncertainty was 0.032 and 0.033, respectively. Uncertainty between MODIS/Aqua VIIRS derived NDVI can be further reduced to 0.022 when aggregating NDVI values over administrative regions. The derived NDVI uncertainties for different MODIS/Aqua and VIIRS products can be used by user community to quantify uncertainties for high level products. With the launch of JPSS-1 VIIRS later this year, there will be a need for additional product inter-comparisons similar to this study, in the context of data inter-use and land long-term data records.

Acknowledgment. This research was funded within the NASA Suomi NPP Science Team, Grant NNX14AR43A. The authors would like to acknowledge Dr. Varaprasad Bandaru for raising a number of considerations in MODIS and VIIRS inter-use.

References

- AghaKouchak, A., A. Farahmand, F. S. Melton, J. Teixeira, M. C. Anderson, B. D. Wardlow, and C. R. Hain. 2015. "Remote sensing of drought: Progress, challenges and opportunities." *Reviews of Geophysics* 53 (2): 452–480.
- Becker-Reshef, I., C. Justice, M. Sullivan, E. Vermote, C. Tucker, A. Anyamba, J. Small *et al.* 2010b. "Monitoring global croplands with coarse resolution earth observations: The Global Agriculture Monitoring (GLAM) project." *Remote Sensing* 2 (6): 1589–1609.

- Becker-Reshef, I., E. Vermote, M. Lindeman, and C. Justice. 2010a. "A generalized regression-based model for forecasting winter wheat yields in Kansas and Ukraine using MODIS data." *Remote Sensing of Environment* 114 (6): 1312–1323.
- Campagnolo, M. L., and E. L. Montano. 2014. "Estimation of effective resolution for daily MODIS gridded surface reflectance products." *IEEE Transactions on Geoscience and Remote Sensing* 52 (9): 5622–5632.
- Campagnolo, M. L., Q. Sun, Y. Liu, C. Schaaf, Z. Wang, and M. O. Román. 2016. "Estimating the effective spatial resolution of the operational BRDF, albedo, and nadir reflectance products from MODIS and VIIRS." *Remote Sensing of Environment* 175: 52–64.
- Chang, J., M. C. Hansen, K. Pittman, M. Carroll, and C. DiMiceli. 2007. "Corn and soybean mapping in the United States using MODIS time-series data sets." *Agronomy Journal* 99 (6): 1654–1664.
- Davies, Diane K., Kevin J. Murphy, Karen Michael, Inbal Becker-Reshef, Christopher O. Justice, Ryan Boller, Scott A. Braun *et al.* "The use of NASA LANCE imagery and data for Near real-time applications." In *Time-Sensitive Remote Sensing*, pp. 165-182. Springer New York, 2015.
- Fan, X., and Y. Liu. 2016. "A global study of NDVI difference among moderate-resolution satellite sensors." *ISPRS Journal of Photogrammetry and Remote Sensing* 121: 177–191.
- Fan, X. and Y. Liu. 2017. "A comparison of NDVI intercalibration methods." *International Journal of Remote Sensing* 38 (19): 5273–5290.
- Franch, B., E. F. Vermote, I. Becker-Reshef, M. Claverie, J. Huang, J. Zhang, C. Justice, and J. A. Sobrino. 2015. "Improving the timeliness of winter wheat production forecast in the United States of America, Ukraine and China using MODIS data and NCAR Growing Degree Day information." *Remote Sensing of Environment* 161: 131–148.
- Franch, B., E. F. Vermote, J.-C. Roger, E. Murphy, I. Becker-Reshef, C. Justice, M. Claverie *et al.* 2017. "A 30+ Year AVHRR Land Surface Reflectance Climate Data Record and Its Application to Wheat Yield Monitoring." *Remote Sensing* 9 (3): 296.
- Gu, Y., J. F. Brown, J. P. Verdin, and B. Wardlow. 2007. "A five-year analysis of MODIS NDVI and NDWI for grassland drought assessment over the central

Great Plains of the United States.” *Geophysical Research Letters* 34 (6): L06407.

- Johnson, D. M. 2016. “A comprehensive assessment of the correlations between field crop yields and commonly used MODIS products.” *International Journal of Applied Earth Observation and Geoinformation* 52: 65–81.
- Johnson, D. M., and R. Mueller. 2010. “The 2009 Cropland Data Layer.” *PE&RS, Photogrammetric Engineering & Remote Sensing* 76 (11): 1201–1205.
- Justice, C. O., M. O. Román, I. Csizsar, E. F. Vermote, R. E. Wolfe, S. J. Hook, M. Friedl *et al.* 2013. “Land and cryosphere products from Suomi NPP VIIRS: Overview and status.” *Journal of Geophysical Research: Atmospheres* 118 (17): 9753–9765.
- Justice, C. O., J. R. G. Townshend, B. N. Holben, and C. J. Tucker. 1985. “Analysis of the phenology of global vegetation using meteorological satellite data.” *International Journal of Remote Sensing* 6 (8): 1271–1318.
- Karl, T. R., B. E. Gleason, M. J. Menne, J. R. McMahon, R. R. Heim, M. J. Brewer, K. E. Kunkel *et al.* 2012. “US temperature and drought: Recent anomalies and trends.” *Eos, Transactions American Geophysical Union* 93 (47): 473–474.
- Kogan, F., N. Kussul, T. Adamenko, S. Skakun, O. Kravchenko, O. Kryvobok, A. Shelestov, A. Kolotii, O. Kussul, and A. Lavrenyuk. 2013. “Winter wheat yield forecasting in Ukraine based on Earth observation, meteorological data and biophysical models.” *International Journal of Applied Earth Observation and Geoinformation* 23: 192–203.
- Kim, Y., A. Huete, T. Miura, and Z. Jiang. 2010. “Spectral compatibility of vegetation indices across sensors: A band decomposition analysis with Hyperion data.” *Journal of Applied Remote Sensing* 4: art num. 043520.
- Meroni, M., D. Fasbender, R. Balaghi, M. Dali, M. Haffani, I. Haythem, J. Hooker *et al.* 2016. “Evaluating NDVI data continuity between SPOT-VEGETATION and PROBA-V missions for operational yield forecasting in North African countries.” *IEEE Transactions on Geoscience and Remote Sensing* 54 (2): 795–804.
- Miura, T., J. P. Turner, and A. R. Huete. 2013. “Spectral compatibility of the NDVI across VIIRS, MODIS, and AVHRR: An analysis of atmospheric effects using EO-1 Hyperion.” *IEEE Transactions on Geoscience and Remote Sensing* 51 (3): 1349–1359.

- Obata, K., T. Miura, H. Yoshioka, A. R. Huete, and M. Vargas. 2016. "Spectral Cross-Calibration of VIIRS Enhanced Vegetation Index with MODIS: A Case Study Using Year-Long Global Data." *Remote Sensing* 8 (1): 34.
doi:10.3390/rs8010034.
- Pahlevan, N., S. Sarkar, S. Devadiga, R. E. Wolfe, M. Román, E. Vermote, G. Lin, and X. Xiong. 2017. "Impact of Spatial Sampling on Continuity of MODIS–VIIRS Land Surface Reflectance Products: A Simulation Approach." *IEEE Transactions on Geoscience and Remote Sensing* 55 (1): 183–196.
- Pittman, K., M. C. Hansen, I. Becker-Reshef, P. V. Potapov, and C. O. Justice. 2010. "Estimating global cropland extent with multi-year MODIS data." *Remote Sensing* 2 (7): 1844–1863.
- Roger, J.-C., E. F. Vermote, S. Devadiga, and Ray, J. P. 2016. "Suomi-NPP VIIRS Surface Reflectance User's Guide." V1 Re-processing (NASA Land SIPS). Accessed 23 June 2017.
https://viirsland.gsfc.nasa.gov/PDF/VIIRS_Surf_Refl_UserGuide_v1.1.pdf.
- Sakamoto, T., B. D. Wardlow, A. A. Gitelson, S. B. Verma, A. E. Suyker, and T. J. Arkebauer. 2010. "A two-step filtering approach for detecting maize and soybean phenology with time-series MODIS data." *Remote Sensing of Environment* 114 (10): 2146–2159.
- Shabanov, N., M. Vargas, T. Miura, A. Sei, and A. Danial. 2015. "Evaluation of the performance of Suomi NPP VIIRS top of canopy vegetation indices over AERONET sites." *Remote Sensing of Environment* 162: 29–44.
- Skakun, S., B. Franch, E. Vermote, J.-C. Roger, I. Becker-Reshef, C. Justice, and N. Kussul. 2017. "Early season large-area winter crop mapping using MODIS NDVI data, growing degree days information and a Gaussian mixture model." *Remote Sensing of Environment* 195: 244–258.
- Tucker, C. J. 1979. "Red and photographic infrared linear combinations for monitoring vegetation." *Remote sensing of Environment* 8 (2): 127–150.
- Vargas, M., T. Miura, N. Shabanov, and A. Kato. 2013. "An initial assessment of Suomi NPP VIIRS vegetation index EDR." *Journal of Geophysical Research: Atmospheres* 118 (22): 12301–12316.
- Van Leeuwen, W., B. J. Orr, S. E. Marsh, and S. M. Herrmann. 2006. "Multi-sensor NDVI data continuity: Uncertainties and implications for vegetation monitoring applications." *Remote Sensing of Environment* 100 (1): 67–81.

- Vermote, E. F., N. Z. Saleous, and C. O. Justice. 2002. "Atmospheric correction of MODIS data in the visible to middle infrared: first results." *Remote Sensing of Environment* 83 (1): 97–111.
- Vermote, E., C. O. Justice, and F.-M. Bréon. 2009. "Towards a generalized approach for correction of the BRDF effect in MODIS directional reflectances." *IEEE Transactions on Geoscience and Remote Sensing* 47 (3): 898–908.
- Vermote, E., C. Justice, and I. Csiszar. 2014. "Early evaluation of the VIIRS calibration, cloud mask and surface reflectance Earth data records." *Remote Sensing of Environment* 148: 134–145.
- Vermote, E. F., and S. Kotchenova. 2008. "Atmospheric correction for the monitoring of land surfaces." *Journal of Geophysical Research: Atmospheres* 113: D23S90. doi:10.1029/2007JD009662.
- Vermote, E. F., J.-C. Roger, and J. P. Ray. May, 2015. "MODIS Surface Reflectance User's Guide. Collection 6." Accessed 23 June 2016. http://modis-sr.ltdri.org/guide/MOD09_UserGuide_v1.4.pdf.
- Wang, D., D. Morton, J. Masek, A. Wu, J. Nagol, X. Xiong, R. Levy, E. Vermote, and R. Wolfe. 2012. "Impact of sensor degradation on the MODIS NDVI time series." *Remote Sensing of Environment* 119: 55–61.
- Whitcraft, A. K., I. Becker-Reshef, and C. O. Justice. 2015. "Agricultural growing season calendars derived from MODIS surface reflectance." *International Journal of Digital Earth* 8 (3): 173–197.
- Xiao, X., S. Boles, J. Liu, D. Zhuang, S. Frolking, C. Li, W. Salas, and B. Moore. 2005. "Mapping paddy rice agriculture in southern China using multi-temporal MODIS images." *Remote Sensing of Environment* 95 (4): 480–492.

Table 1. The M{O,Y}D09 Collection 6 Product Suite (Vermote *et al.* 2015).

Product name (Terra / Aqua)	Product description
MOD09GQ / MYD09GQ	Surface Reflectance Daily L2G Global 250 m (bands 1, 2)
MOD09GA / MYD09GA	Surface Reflectance Daily L2G Global 500 m and 1 km (bands 1–7)
MOD09Q1 / MYD09Q1	Surface Reflectance 8-Day L3 Global 250 m (bands 1, 2)
MOD09A1 / MYD09A1	Surface Reflectance 8-Day L3 Global 500 m (bands 1–7)
MOD09CMG / MYD09CMG	Surface Reflectance Daily L3 Global 0.05° CMG (bands 1–7)

Table 2. The VNP09 Collection 1 Product Suite (Roger *et al.* 2016).

Product name	Product description
VNP09GHKI	Surface Reflectance Daily L2G Global 500 m (bands I1–I3)
VNP09GIKI	Surface Reflectance Daily L2G Global 1 km (bands M1–M5, M7, M8, M10, M11)
VNP09GA	Surface Reflectance Daily L2G Global 500 m and 1 km (bands I1–I3 (500m), M1–M5, M7, M8, M10, M11 (1 km))
VNP09A1	Surface Reflectance 8-Day L3 Global 500 m (bands I1–I3)
VNP09H1	Surface Reflectance 8-Day L3 Global 1 km (bands M1–M5, M7, M8, M10, M11)

VNP09CMG	Surface Reflectance Daily L3 Global 0.05° CMG (bands I1–I3, M1–M5, M7, M8, M10, M11)
----------	---

Table 3. Estimated conversion coefficients for spectral adjustment of red and NIR spectral bands from VNP09A1 to MYD09A1. Only pixels with the same DOY and close to nadir observations ($VZA < 7.5^\circ$) for MYD09A1 and VNP09A1 were considered.

Period	a_{red}	b_{red}	a_{NIR}	b_{NIR}
2012	0.9788	0.0174	0.0834	0.9394
2013	0.9704	0.0185	0.0778	0.9417
2014	0.9628	0.0204	0.0357	0.9622
2015	0.9691	0.0196	0.0378	0.9622
2016	0.9562	0.0176	0.0369	0.9533
Mean \pm standard deviation (coefficient of variation, %)	0.9674 \pm 0.0085 (0.9%)	0.0187 \pm 0.0013 (6.8%)	0.0543 \pm 0.0241 (44.3%)	0.9518 \pm 0.0109 (1.1%)
2012-2016	0.9687	0.0184	0.0544	0.9518

Table 4. Estimated coefficients for spectral adjustment of red and NIR spectral bands from MYD09CMG and VNP09CMG.

Period	a_{red}	b_{red}	a_{NIR}	b_{NIR}
2012	0.9805	0.0187	0.0011	0.9720
2013	0.9812	0.0190	0.0008	0.9733
2014	0.9799	0.0189	0.0011	0.9724
2015	0.9809	0.0184	0.0010	0.9730
2016	0.9842	0.0143	0.0010	0.9730
Mean \pm standard deviation (coefficient of variation, %)	0.9813 \pm 0.0017 (0.2%)	0.0178 \pm 0.0020 (11.2%)	0.0010 \pm 0.0001 (10.8%)	0.9727 \pm 0.0005 (0.1%)
2012-2016	0.9814	0.0178	0.0020	0.9717

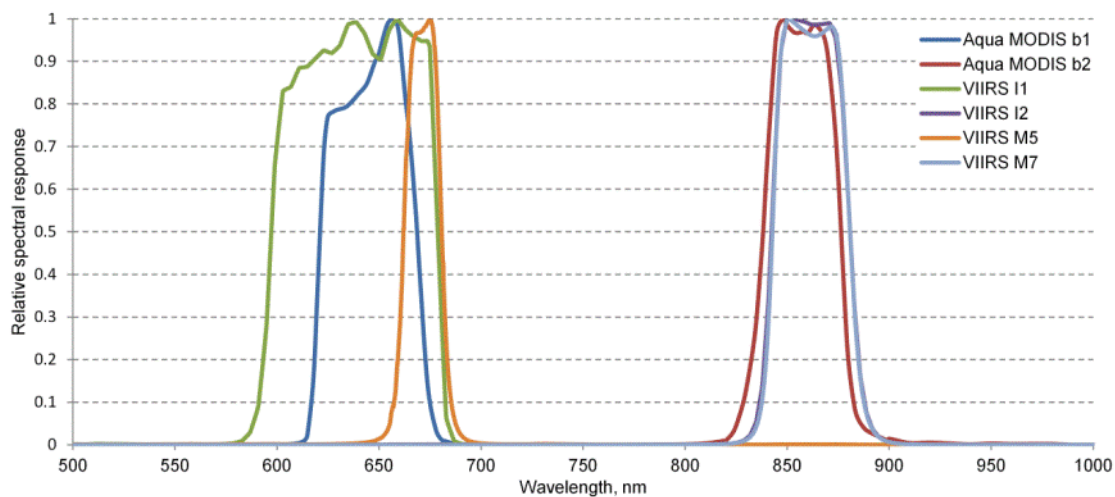


Figure 1. Relative spectral response functions for MODIS/Aqua and VIIRS sensors in the red and NIR spectral domain. The functions for MODIS and VIIRS were derived from <https://mcst.gsfc.nasa.gov/calibration/parameters> and <https://ncc.nesdis.noaa.gov/VIIRS/VIIRSSpectralResponseFunctions.php>, respectively.

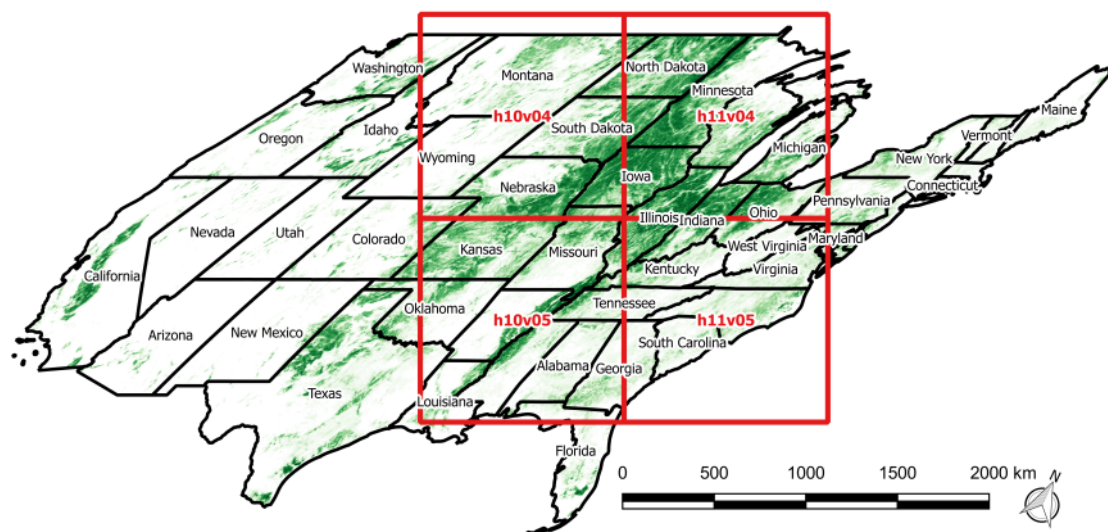


Figure 2. Illustration of four MODIS tiles over the US (in MODIS sinusoidal projection) used for comparison of 500 m 8-day composite products from MODIS (MYD09A1) and VIIRS (VNP09A1) sensors. Shown also is a distribution of croplands derived from the USDA's Cropland Data Layer (CDL) for 2016 (Johnson and Mueller 2010).

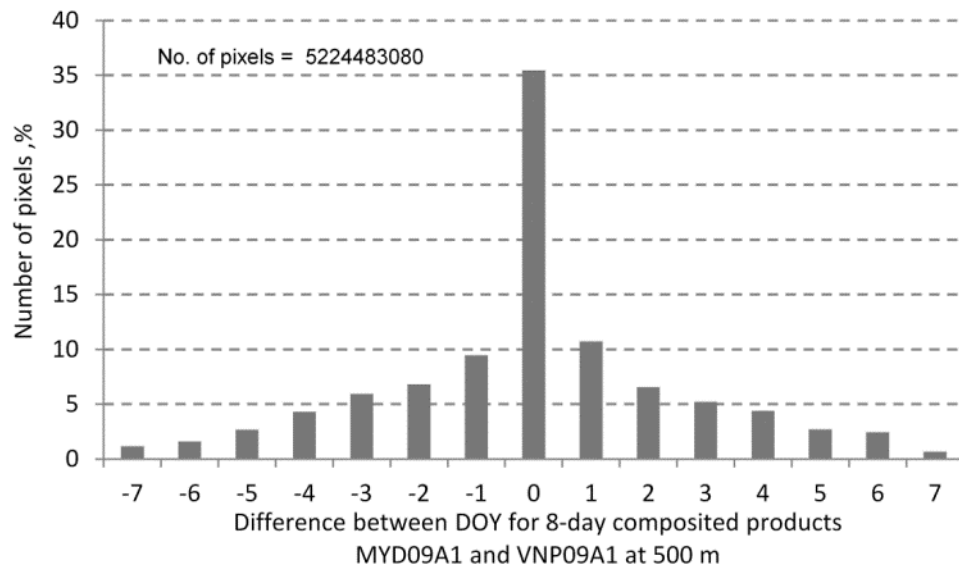


Figure 3. Distribution of DOY difference for MYD09A1 and VNP09A1 8-day composite products at 500 m spatial resolution. All land pixels from MODIS tiles h10v04, h10v05, h11v04 and h11v05 for 2012–2016 were used to build the chart.

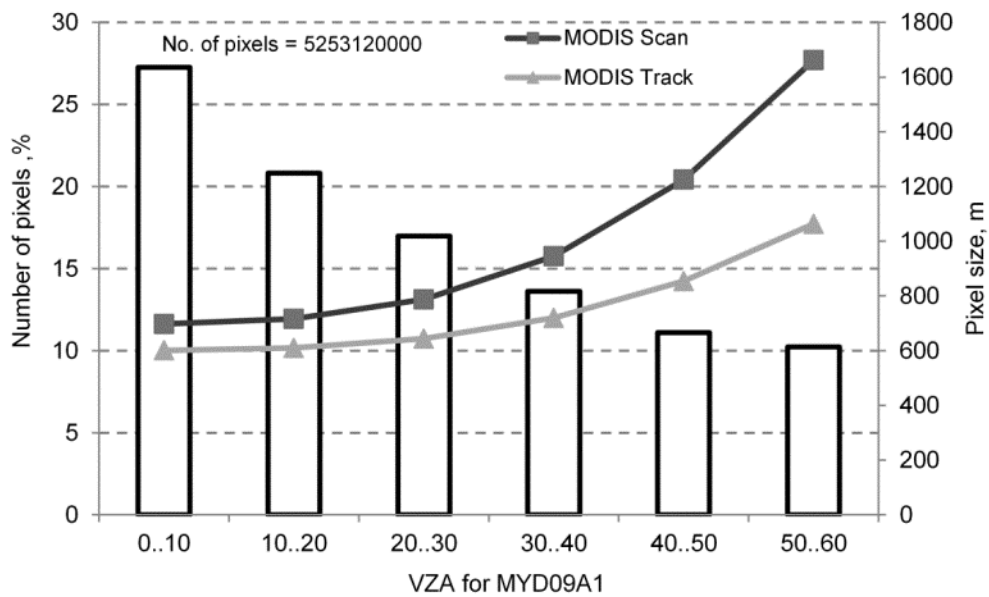


Figure 4. Distribution of VZA values for ‘best pixels’ selected within the 8-day period for the MYD09A1 products. All land pixels from MODIS tiles h10v04, h10v05, h11v04 and h11v05 for 2012–2016 were used to build the chart. Also shown are the effective MODIS along-scan and along-track pixel sizes for the nominal 500 m resolution depending on VZAs (Campagnolo and Montano 2014).

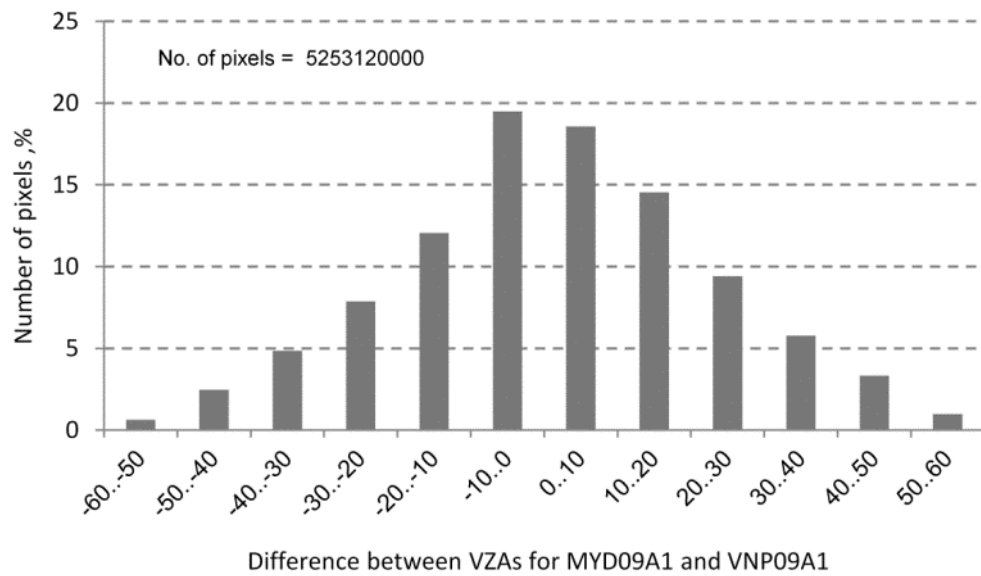


Figure 5. Distribution of the difference between VZA values for MYD09A1 and VNP09A1 8-day composite products at 500 m spatial resolution. All land pixels from MODIS tiles h10v04, h10v05, h11v04 and h11v05 for 2012–2016 were used to build the chart.

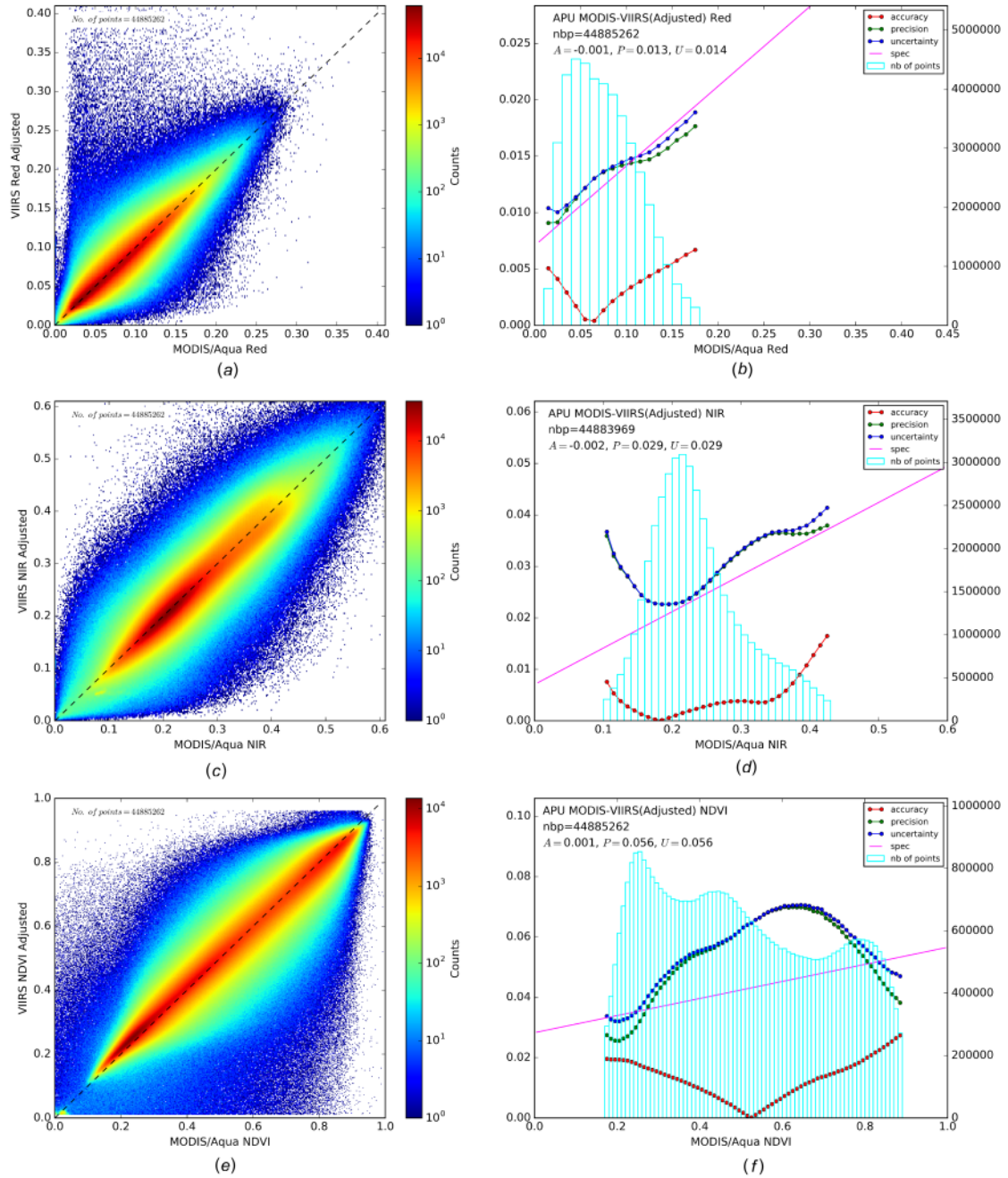


Figure 6. A scatterplot of red, NIR and NDVI values derived from VNP09A1 (after spectral adjustment) and MYD09A1 at 500 m resolution (a), (c) (e). Corresponding APU analysis (b), (d) (f). Land pixels from MODIS tiles h10v04, h10v05, h11v04 and h11v05 for 2012–2016 and having the same DOY for MODIS and VIIRS and close to nadir observations ($VZAs < 7.5^\circ$) were considered. The light blues bars on (b), (d) (f) show the number of points used in each bin of surface reflectance or NDVI values from MODIS/Aqua (used as a reference). The APU values (Equations (6)–(8)) were computed for points in each bin and being shown in red (accuracy), green (precision)

and blue (uncertainty). The pink represents the specified uncertainty based on theoretical error budget of the Collection 5 MODIS (Vermote and Kotchenova 2008): $\sqrt{2}(0.005 + 0.05\rho)$ for spectral bands and $\sqrt{2}(0.02 + 0.02VI)$ for NDVI. The $\sqrt{2}$ term is used since we are focusing on inter-consistency of datasets and not validation.

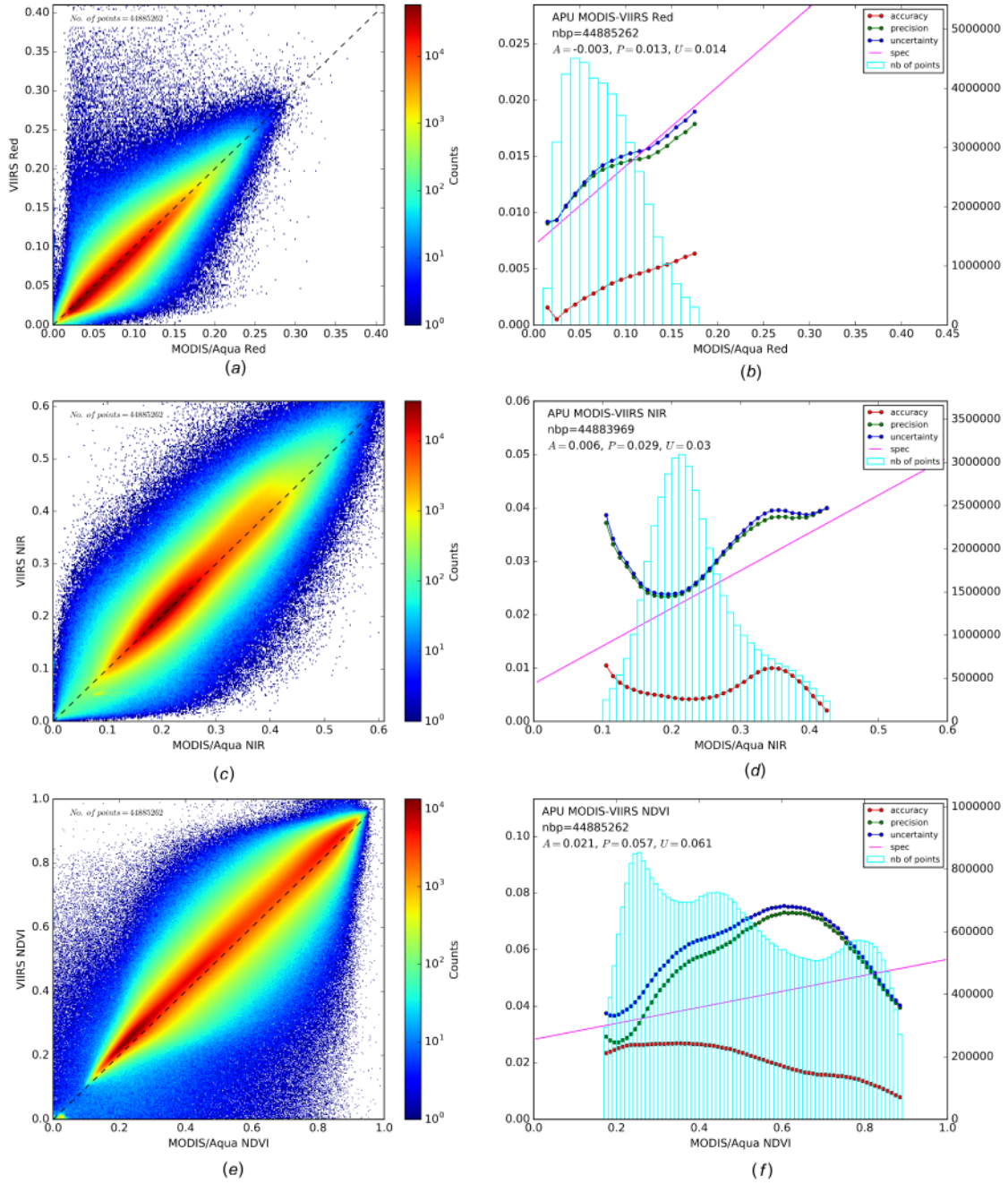


Figure 7. The same as Figure 6 but without spectral adjustment.

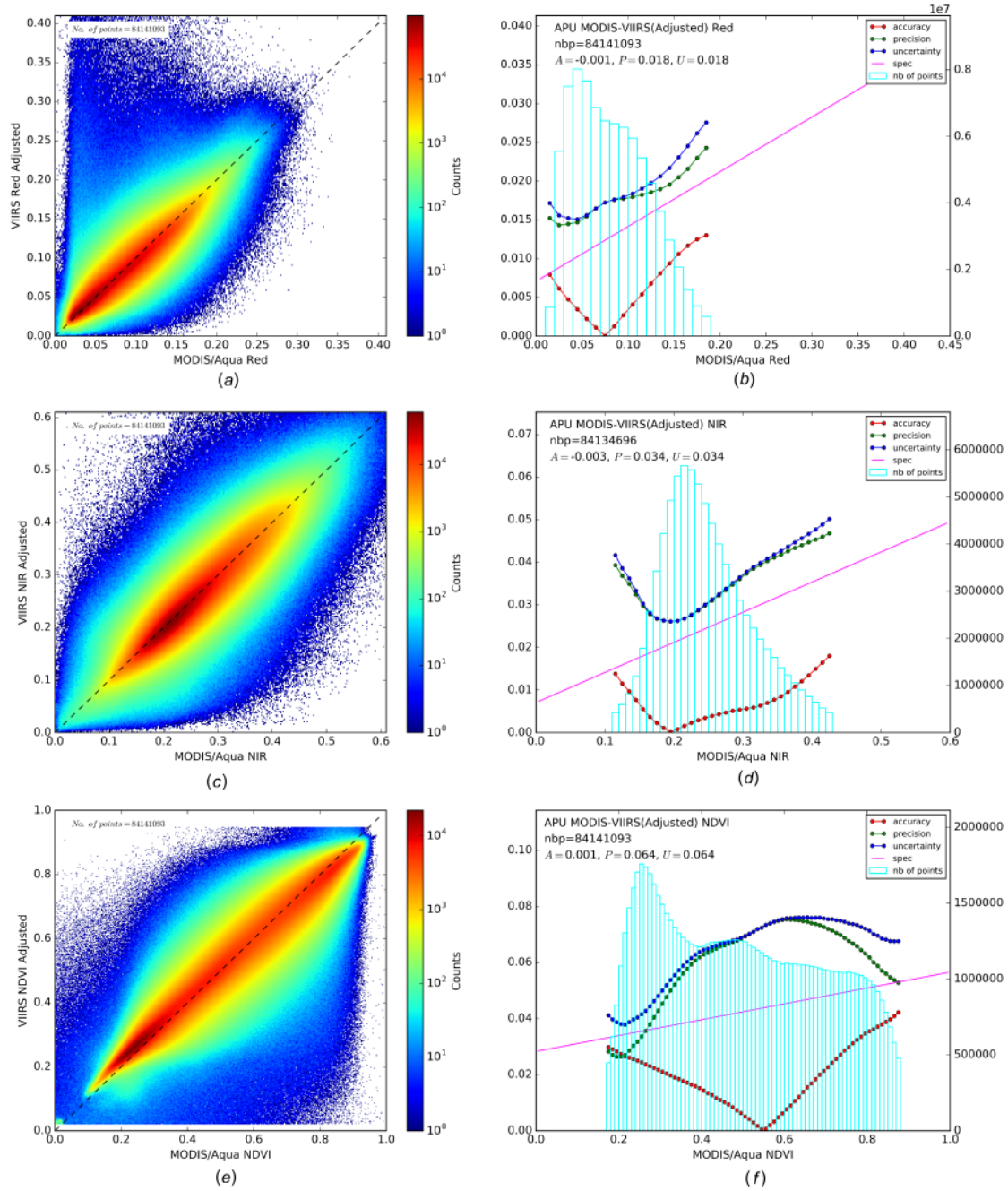


Figure 8. The same as Figure 6 but the absolute difference between DOY for MYD09A1 and VNP09A1 is 3 to 7 days.

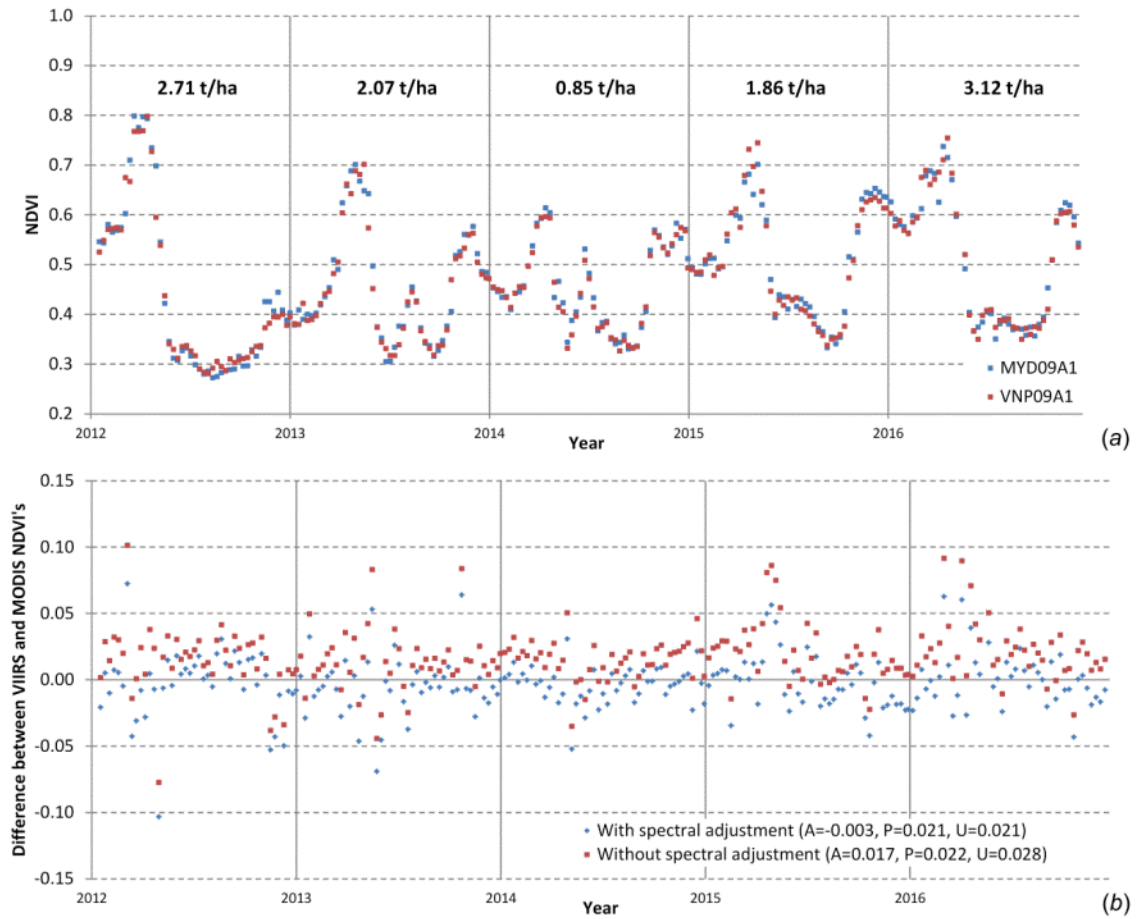


Figure 9. A time series of NDVI values derived from MYD09A1 and VNP09A1 8-day products at 500 m resolution for Harper County, one of the largest wheat producing counties in Kansas. Surface reflectance values in red and NIR bands, that were used to compute NDVI from VIIRS, were spectrally adjusted to match the MODIS/Aqua ones (using Equations (2)–(3) and derived coefficients from Table 3). Shown also are final winter wheat yields derived from USDA National Agricultural Statistics Service (NASS) statistics (a). The difference between aggregated NDVI values from MYD09A1 and VNP09A1 with and without spectral adjustment of the VIIRS bands (b).

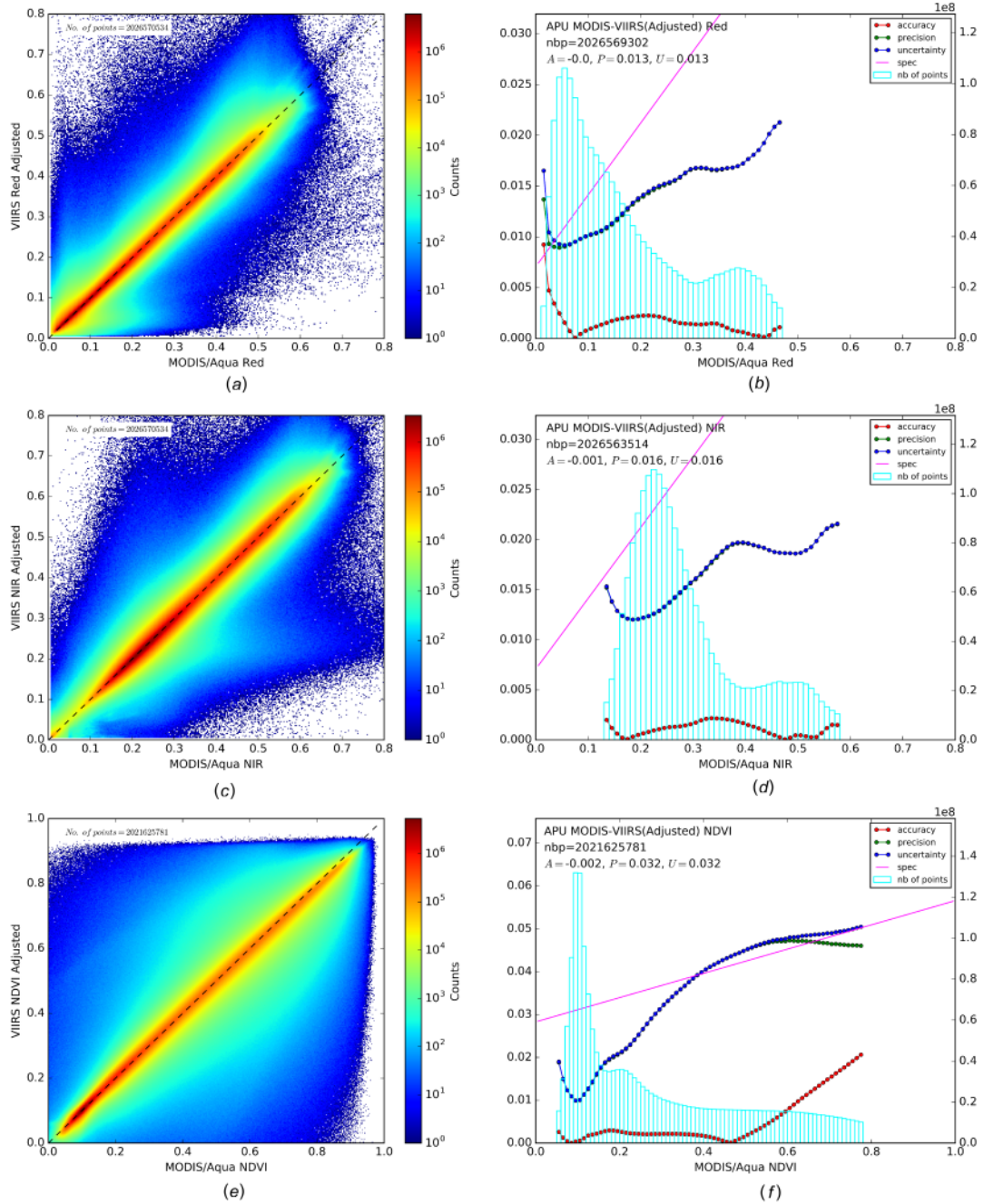


Fig. 10. A scatterplot of red, NIR and NDVI values derived from VNP09CMG (after spectral adjustment) and MYD09CMG at 0.05° resolution (a), (c) (e). Corresponding APU analysis (b), (d) (f). The light blues bars on (b), (d), (f) show the number of points used in each bin of surface reflectance or NDVI values from MODIS (used as a reference). The APU values (Equations (6)–(8)) were computed for points in each bin and being shown in red (accuracy), green (precision) and blue (uncertainty). The pink represents the specified uncertainty based on theoretical error budget of the Collection 5 MODIS NDVI (Vermote and Kotchenova 2008).

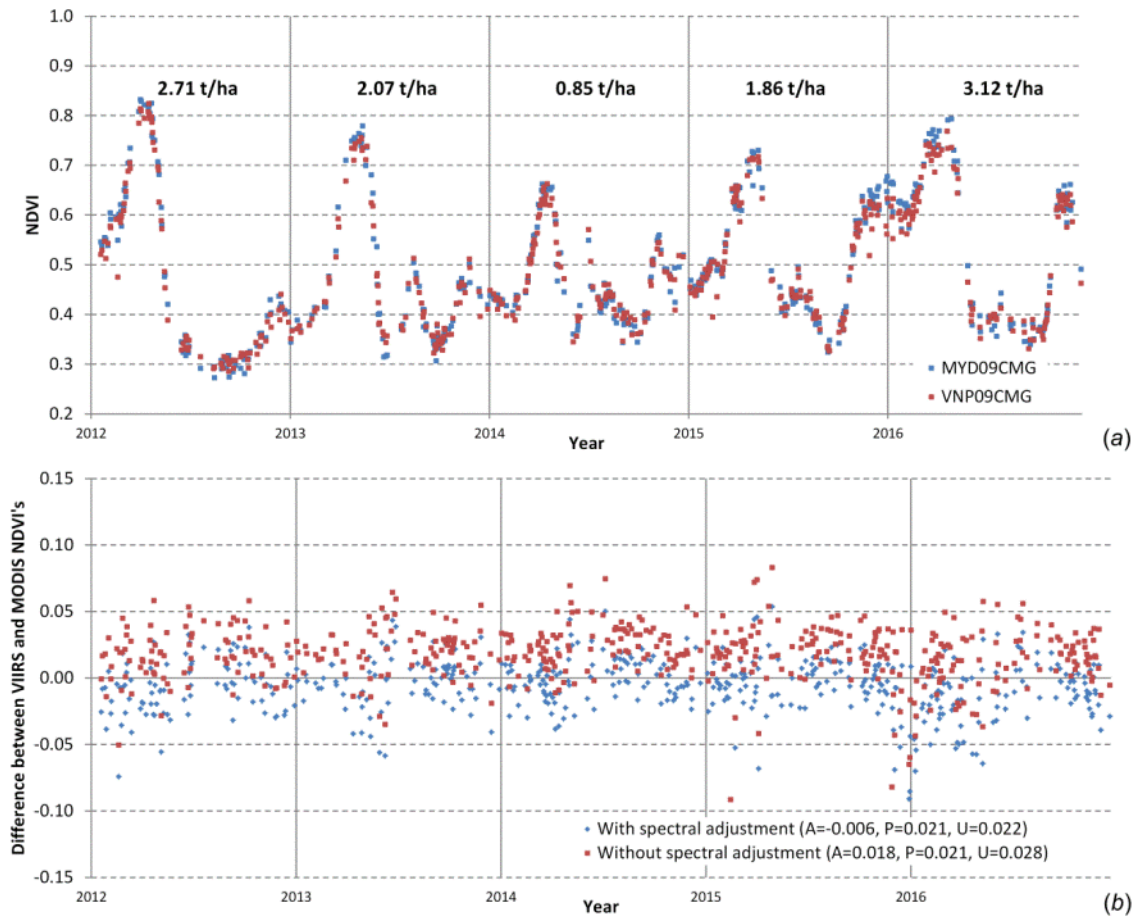


Figure 11. A time series of NDVI values derived from BRDF corrected MYD09CMG and VNP09CMG daily products at 0.05° resolution for Harper County. Surface reflectance values in red (I1) and NIR (I2) bands, that were used to compute NDVI from VIIRS, were spectrally adjusted to match the MODIS/Aqua ones. Shown also are final winter wheat yields derived from USDA NASS statistics (a). A difference between aggregated NDVI values from MYD09CMG and VNP09CMG with and without spectral adjustment for VIIRS bands (b).

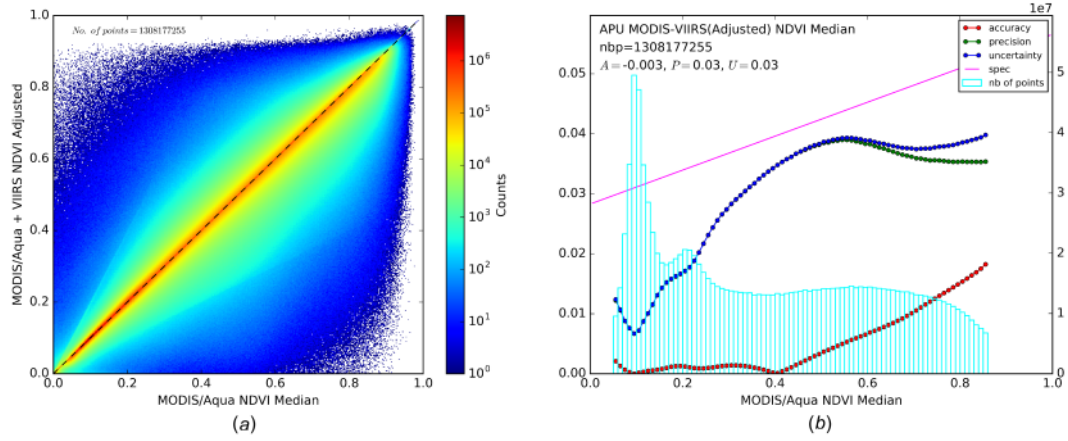


Figure 12. Comparison of median NDVI values at CMG resolution derived from MODIS/Aqua (Equation (4)) and a combination of MODIS/Aqua and adjusted VIIRS (Equation (5)) for 2002–2016 at a daily timestamp. A combined (MODIS/Aqua and VIIRS) median NDVI versus MODIS/Aqua derived median NDVI is shown in (a); APU analysis (b).

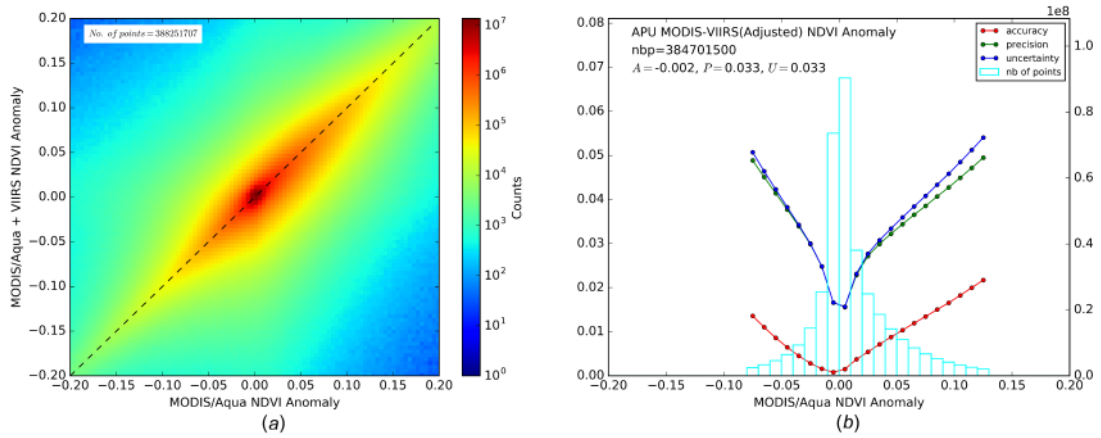


Figure 13. Comparison of NDVI anomalies for 2016 at CMG resolution at daily timestamp. Anomalies were derived by subtracting daily NDVI values for 2016 from median values calculated for 2002–2015. Combined (MODIS/Aqua and VIIRS) NDVI anomalies versus MODIS/Aqua derived NDVI anomalies is shown in (a); APU analysis (b).

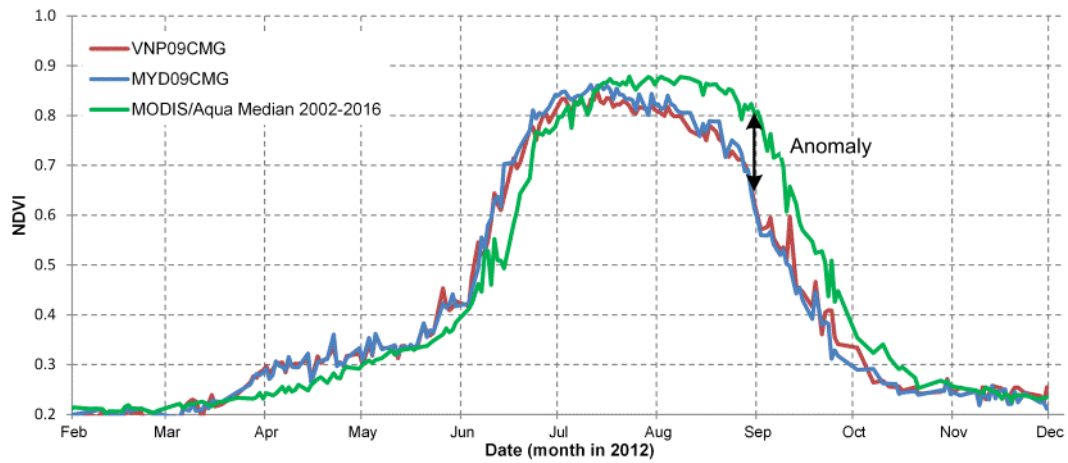


Figure 14. Corn growth dynamics derived from MODIS/Aqua and VIIRS in 2012 in Iowa (US) compared to the median NDVI values for 2002–2016 derived from MODIS/Aqua. Due to a drought, corn growth started to decrease significantly from June which resulted in a 25% yield reduction according to USDA NASS.

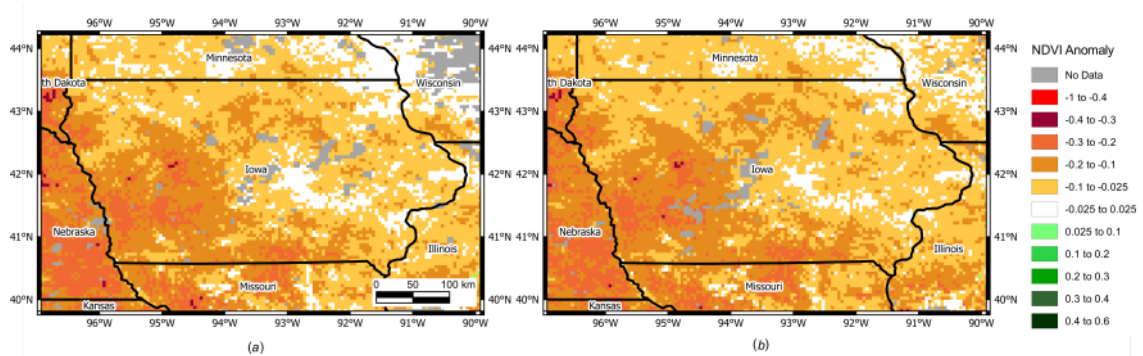


Figure 15. NDVI anomalies at 0.05° spatial resolution for the state of Iowa (US) derived from MODIS/Aqua (a), and adjusted VIIRS (b) data on 21 August 2012. Anomalies were computed by subtracting NDVI values from the median NDVI values for 2002–2016 derived from MODIS/Aqua.

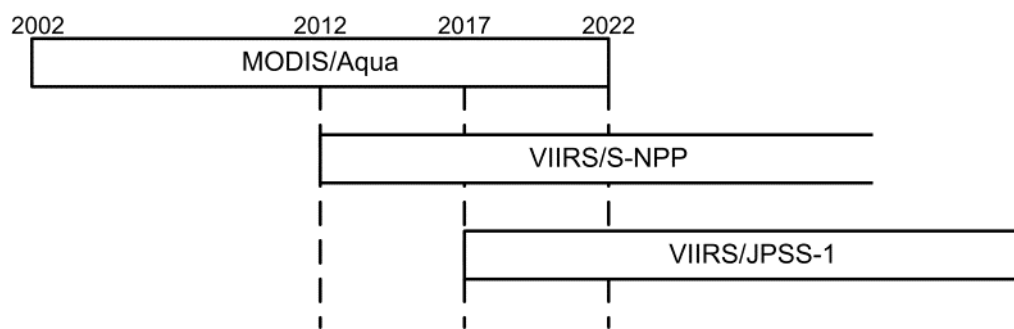


Figure 16. Timeline of the three afternoon remote sensing satellites: Aqua, S-NPP and JPSS-1.